The Role of Sea Spray in Cleansing Air Pollution over Ocean via Cloud Processes

Daniel Rosenfeld, Ronen Lahav, Alexander Khain, Mark Pinsky

Particulate air pollution has been shown to strongly suppress precipitation from convective clouds over land. New observations show that precipitation from similar polluted clouds over oceans is much less affected, because large sea salt nuclei override the precipitation suppression effect of the large number of small pollution nuclei. Raindrops initiated by the sea salt grow by collecting small cloud droplets that form on the pollution particles, thereby cleansing the air. Therefore, sea salt helps cleanse the atmosphere of the air pollution via cloud processes. This implies that over oceans, the climatic aerosol indirect effects are significantly smaller than current estimates.

Huge amounts of air pollution spill off the South Asian continent over the Indian Ocean and spread all the way to the intertropical convergence zone (ITCZ). These aerosols are composed of a mixture of smoke from biomass burning, urban air pollution, and desert dust (*1*), all of which act to suppress precipitation (*2–4*) by providing large concentrations of small cloud condensation nuclei (CCN). Indeed, aircraft measurements in small trade-wind clouds over the Indian Ocean showed that the average droplet concentration in clouds feeding on the polluted air was 315 cm^{-3}, whereas in pristine air it was only 89 cm^{-3}. Drizzle concentration in polluted air was suppressed to 25% of the value in pristine air (*5*). We wanted to see how these observations in shallow clouds might translate to the suppression of precipitation in the deeper convective clouds, using methods similar to those previously applied to clouds forming in polluted air over land (*2–4*), and what happens when the clouds advect over the ocean toward the ITCZ.

Observations. According to measurements from the Tropical Rainfall Measuring Mission (TRMM) satellite, clouds in the polluted air over land had a droplet effective radius (r_{eff}) smaller than the precipitation threshold of 14 μm (*6*) and did not develop radar precipitation echoes when their tops were below the −10°C isotherm level (black curve in Fig. 1), which was at a height of about 6 km. This effect of precipitation suppression over land was recently simulated by Khain *et al.* (*7*) using a spectral-microphysics cloud model.

The amount of pollution in the air did not diminish much when it moved over the sea for many hundreds of kilometers, as indicated by the consistent observed turbidity of the air (Figs. 1 and 2). This can be related to the CCN concentration (*8*). However, clouds developing in the polluted air over the sea had larger r_{eff} than clouds of the same depth over land, and this was increasingly true further away from land (Fig. 1). The TRMM measurements show that, unlike polluted clouds over land, deep clouds developing in polluted air over the ocean behaved like maritime clouds, with rainout signature [that is, the air goes up, but the rain forms quickly and falls through the updraft (*9*)] and with high glaciation temperature as inferred from the indicated r_{eff} reaching its saturation value near −10°C. The TRMM precipitation radar showed (Fig. 1) that clouds over the sea almost always precipitated at intensities $>\sim 1$ mm $hour^{-1}$ when their tops exceeded the height of 3 km (about 10°C isotherm), with no obvious differences in the precipitation echoes from clouds forming in the polluted or pristine air. The observation that the r_{eff} at a given cloud depth [depth is represented by temperature (T) minus T at the bottom of the T-r_{eff} curve, which is lower by 1 to 2 K than the actual cloud base temperature] was smaller at shorter distance over the sea downwind from the pollution source suggests that the pollution particles affected the cloud microstructure to produce smaller droplets, but unlike the case over land, this did not seem to appreciably suppress the precipitation in the clouds over the ocean.

There are two potentially relevant differences between land and ocean that may help explain why deep clouds react so differently to pollution over land and over ocean. First, sea spray forms large (>1 μm in diameter) sea salt aerosols, which are the first to form droplets at the cloud base, thereby reducing the supersaturation there and preventing the activation of smaller pollution aerosols into cloud droplets (*10–15*). This reduces the droplet number-concentration and leads to enhanced coalescence, which can progress sufficiently to form rain in convective clouds deeper than about 3 km. Second, updraft velocities over ocean are weaker than over land; therefore, a smaller fraction of the aerosols is nucleated into cloud droplets (*16*, *17*). In addition, more time is available for the coalescence to progress and form warm precipitation.

Satellite inferences. Additional satellite analyses of clouds occurring in polluted air masses moving from Thailand to the Bay of Bengal (Fig. 3) provided insight into the relative importance of these two potential explanations. An area of clouds with elevated base over the Andaman Sea, as evident from the largest T of curve B, had the same small r_{eff} as the clouds upwind over land (curve A). When low-level clouds formed in addition to the high-base clouds, the r_{eff} increased, especially near the base (curve C). Further downwind, when the clouds with elevated base disappeared and all the clouds were fed from the low-level base, the r_{eff} increased further with decreasing T or increasing height (curve D). The r_{eff} further increased downwind toward the ITCZ and beyond (Fig. 1).

A possible explanation of these observations would be that the air pollution from the land overrides a cleaner marine air near the surface. However, according to back-trajectory analysis using the National Oceanic and Atmospheric Administration (NOAA)–HYSPLIT model (*18*), the wind direction was from the land at the surface level. The aerosol optical depth (AOD) was about 0.35, and ship aerosol and light detection and ranging (LIDAR) measurements showed that the pollution was generally confined to the lowest 3 km and reached the surface (*1*, *19*). Another possible explanation is that the updraft velocity at the cloud base forms smaller droplets for greater upward velocities. However, the elevated clouds seem in the TRMM satellite imagery to be less convective than the clouds with the lower bases and therefore highly unlikely to have greater updrafts at the cloud base or higher. The remaining possible explanation is the presence of large sea salt CCN at the marine boundary layer of the atmosphere, but not at the higher levels or over land.

Sea salt aerosols that originate from sea spray are known to be added to the air mass during travel over the ocean, at a size distribution that is closely related to the surface wind velocity (*20*). LIDAR measurements (*21*) show that the sea salt particles are nearly evenly distributed within the mixed layer up to the cloud base, where they are ingested with the updrafts into the clouds. We suggest here that the observed enlargement of r_{eff} at low levels (see curve C in Fig. 3) was due to low-level clouds ingesting the sea spray. The higher clouds had smaller r_{eff} because they ingested air from above the marine boundary layer that contained air pollution without sea spray.

Albrecht (*22*) noted that drizzle develops

Institute of Earth Sciences, the Hebrew University of Jerusalem, Jerusalem 91904, Israel.

in stratocumulus clouds containing droplet concentrations of less than about 150 drops cm^{-3} and with droplet radii $>\sim 15$ μm. He also recognized that the drizzle washes out the CCN and so causes the subsequent clouds to contain smaller concentrations of larger drops, thereby creating more favorable conditions for drizzle, establishing a positive feedback loop. In the extreme situation, this leads to elimination of all the CCN and to collapse of the marine boundary layer and dissipation of the clouds (*23*). Conversely, shallow stratocumulus clouds in polluted air develop very little drizzle, so that little pollution is washed down.

Cloud simulations. According to the TRMM Precipitation Radar (PR), polluted tropical clouds over land start precipitating when their tops reach the −10°C isotherm, which is at about 6 to 6.5 km. This was found to be the case over Indonesia (*2*) and the Amazon (*24*) as well as in southern India (curve A of Fig. 1). Apparently, the height that polluted cloud tops have to exceed to initiate precipitation is much smaller over ocean (~3 km or 10°C isotherm) than over land. The PR does not detect precipitation in clouds much lower than 3 km even in pristine conditions, because they produce mainly small raindrops (*25*) that do not reflect echoes above the PR detection threshold (~17 dBZ at a 4-km footprint).

The greater updraft velocities over land can also explain differences between land and ocean in cloud droplet concentrations, coalescence, and precipitation. This requires further quantitative investigation, which was done using a one-dimensional warm rain cloud parcel model (*26*). The model has 2000 size bins for CCN and drops, to obtain high accuracy for the nucleation and diffusional growth of cloud droplets and for the coalescence process.

The aerosols were taken from the measurements of NOAA's research vessel *Ron Brown* in the Indian Ocean during February and March 1999. Four spectra were extracted to encompass the range of variability: (i) pristine maritime, at Julian day 79.271 near the southern edge of the cruise, in little-polluted maritime air to the south of the ITCZ, denoted as "Clean" in Fig. 4; (ii) polluted air over the sea near the northern edge of the cruise, at Julian day 69.25, denoted as "Polluted" in Fig. 4; and polluted air of the second spectrum but with sea spray truncated to Junge distribution at radii (iii) 0.3 μm and (iv) 0.6 μm, denoted as "Pol, $R < 0.3$" and "Pol, $R < 0.6$," respectively, in Fig. 4.

The measured aerosol spectra were converted to NaCl equivalent particles according to the following procedure: Aerosols with a diameter smaller than 1 μm were assumed to be mostly pollution particles and were assumed to contain 15% equivalent of NaCl. Aerosols with a diameter greater than 1 μm were assumed to be exclusively composed of sea spray and were left as is. This is justified by selecting the polluted case with large aerosols in concentrations that do not exceed those of the maritime case, where the aerosols >1 μm can be assumed to be exclusively sea salt. Polluted aerosols over land, without sea spray, were simulated by replacing the large aerosols having diameter greater than 0.6 or 1.2 μm by Junge distribution.

The simulations replicated the observation (*6*) of r_{eff} near 14 μm as a precipitation threshold. The tops of simulated polluted clouds without sea spray have to exceed the height of 5 km to start precipitating, but the addition of the sea spray reduced that height to 3 km; unpolluted clouds start developing significant precipitation at 2.3 km. There is little sensitivity to the exact size of the truncation of the sea spray. This means that the larger sea spray particles are dominating the restoration of the precipitation in the polluted clouds.

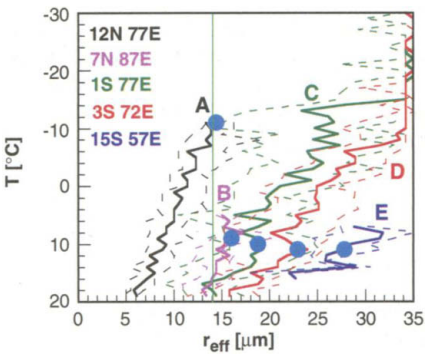

Fig. 1. The relation between T and r_{eff} as observed by the TRMM satellite in deep convective clouds occurring in (curve A) heavily polluted air over south India on 24 March 1999; (curve B) polluted air in the northeasterly trade winds on 11 February 1999, with median TRMM AOD of 0.35, (curve C) in air reaching the northern rain band of the ITCZ with AOD = 0.27, (curve D) and in air to the south of the northern cloud band of the ITCZ, still in the Northern Hemisphere air mass, with AOD = 23; (curve E) and lastly in the Southern Hemisphere pristine trade winds, with AOD = 0.07. Plotted are the 50th (solid lines), 15th, and 85th (dashed lines) percentiles of r_{eff} for each 1 K interval. The vertical green line marks the precipitation threshold of 14 μm. The blue dots denote the lowest cloud-top temperature that still contained detectable TRMM radar precipitation echoes. r_{eff} is less than 14 μm over land, so that precipitation is completely suppressed there below the −10°C isotherm, whereas deep clouds in polluted air over the sea (curve B) precipitate readily, with some further decreasing threshold depth further to the south (curves C to E) in the cleaner clouds.

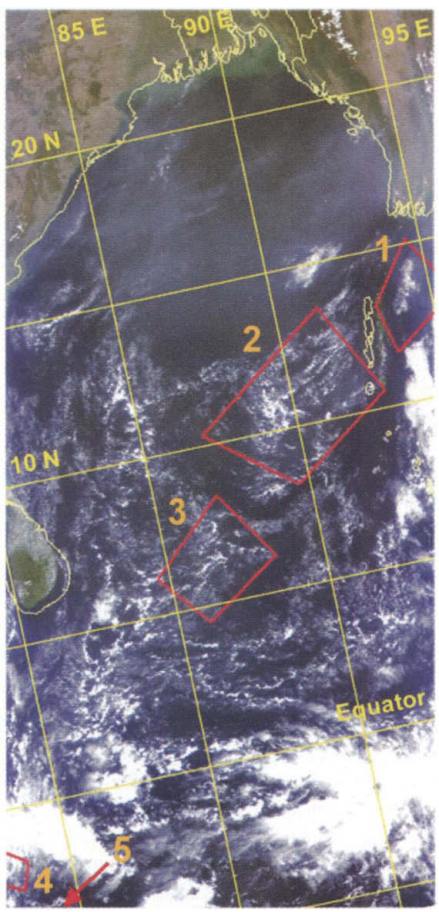

Fig. 2. Sea-viewing Wide Field-of-view Sensor (SeaWiFS) image of clouds forming in polluted air flowing toward the ITCZ, over the Bay of Bengal and the Indian Ocean to its south, on 11 February 1999, 07:39 Greenwich mean time, about 2 hours after the TRMM overpass. Frames 1, 2, and 3 correspond to curves B, C, and D of Fig. 3, respectively. Frames 3, 4, and 5 (5 is outside the image in the direction of the arrow) correspond to curves B, C, and D of Fig. 1.

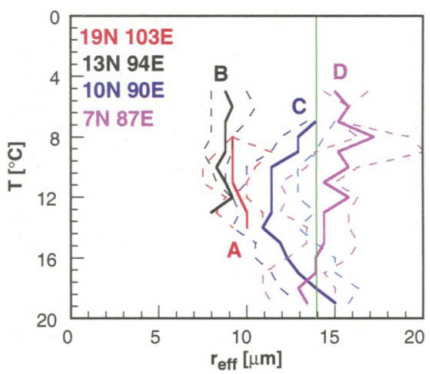

Fig. 3. T-r_{eff} relations as in Fig. 1, for clouds developing in (curve A) heavily polluted air over north Thailand on 11 February 1999, moving to the (curve B) north Bay of Bengal and forming elevated-base clouds with small r_{eff}; but when clouds with low bases are added (curve C), the lower (warmer) clouds have much larger r_{eff} values that (curve D) expand to the whole cloud depth when only the low-base clouds remain. AOD = 0.35 in areas C and D. r_{eff} continues growing further downwind, as shown in Fig. 1.

The simulated cloud base updraft was 1 m s^{-1}, and the vertical velocity increased with height, reaching a maximum of 9 m s^{-1} at the height of 5 km. These are typical vertical velocities for the maritime environment but smaller than typical for continental convective clouds. Additional simulations (Fig. 5) tested the sensitivity of the height of precipitation initiation to the cloud base updraft. As expected, all heights shown in Fig. 4 increased with greater updraft velocities, but the relative changes remained similar. The higher base of clouds over land and the greater cloud base updrafts that typically occur there can explain the observation of clouds exceeding 6.5 km in height before they start precipitating (curve A in Fig. 1) (*2*, *24*).

The sea spray in the polluted air decreased the maximum cloud base supersaturation and hence reduced the droplet concentrations. Buildup of greater supersaturation higher in the cloud caused additional CCN to nucleate cloud droplets. This increase in supersaturation is observed in the area of active coalescence that leads to a decrease in drop concentration within cloud updraft. This explains the sudden increase in the drop concentration with height shown for the curve of the polluted air with sea salt in Fig. 4B. The renewed nucleation of small droplets aloft in the polluted air with sea spray can explain the observed smaller r_{eff} aloft in the precipitating clouds that form closer to the pollution source (see the r_{eff} above the blue dots in Fig. 1).

The simulated drop concentrations should be compared to the peak concentrations in the aircraft measurements, which represent the undiluted parcel at the cores of the updrafts. The peak concentrations are roughly double the average concentrations. Given that, there is a reasonable agreement between the model results and the aircraft-measured average drop concentrations (*5*).

Conclusions. The winter monsoon is a flow of cool and highly polluted air mass off the Southeast Asian continent to the relatively warm waters of the ocean. The polluted clouds over land need to grow beyond 6 km in height to start precipitating. The warming and moistening of the air at the sea surface as it flows toward the ITCZ causes cumulus convection, with cloud tops often reaching 3 km, becoming gradually deeper with the approach to the ITCZ. According to simulations that take into account the effects of lower cloud bases and updrafts over the sea, the particulate air pollution would still have caused these convective clouds to become microphysically "continental" and avoid precipitating at heights less than 4 km. However, the sea spray "seeds" the clouds over the sea and affects them in two ways: It provides large CCN that create initial larger cloud droplets that initiate the coalescence processes, and it decreases the maximum supersaturation at the cloud base, and so prevents the nucleation of the smaller pollution particles into cloud drops. This reduces the cloud drop number-concentration and increases their size, leading to enhanced precipitation.

The bulk of the cloud droplets are nucleated on the larger pollution particles. The much larger sea spray particles add only a small number of large droplets that collect the smaller polluted droplets and eventually precipitate them as raindrops. In the final account, the sea spray cleanses the atmosphere of pollution particles that nucleated cloud droplets. The second generation of clouds that forms in the air is already cleaner, with smaller numbers of droplets and thus more efficient coalescence and further cleansing by rainfall. This constitutes a positive feedback loop that leads to the formation of pristine maritime air masses.

This cleansing process would advance more slowly in shallower clouds, because a minimum depth is required to form substantial precipitation, which according to the cloud simulation here is about 3 km for the marine polluted clouds (Fig. 4). The best conditions for cleansing air pollution over the sea would be deep clouds and high surface winds that raise much sea spray. However, in the case of smaller concentrations with weaker winds, the added travel time would compensate for the slower cleansing processes. If the oceans were not salty, air pollution would remain for much longer in the lower troposphere and would spread to much greater areas of the oceans. The clouds would have to grow vertically to about 5 km to initiate substantial precipitation in polluted air over a hypothetical salt-free ocean. This height is well above the tops of common convective clouds even under elevated subtropical inversion. Therefore, such deeper clouds cover much smaller areas of the oceans, leaving a major role for sea spray in making the difference between nonprecipitating and precipitating clouds.

This has important climate implications: Maritime clouds have been considered to be the

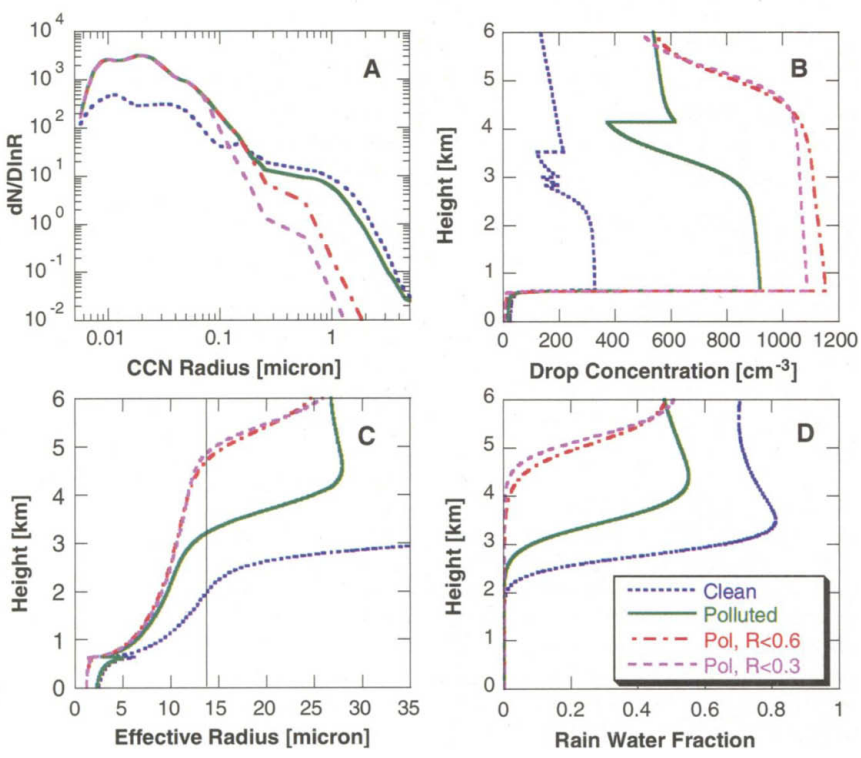

Fig. 4. Simulations of clouds with CCN aerosol size distributions in equivalent-solubility dry NaCl particles, for clean air with sea spray (SS), polluted air with SS, and polluted air with SS truncated above radii of 0.3 and 0.6 μm, shown in (**A**). The concentration of drops with radius >0.5 μm (**B**), effective drop radius (**C**), and fraction of cloud water converted to raindrops (**D**) are shown as a function of height for the four aerosol spectra in (A).

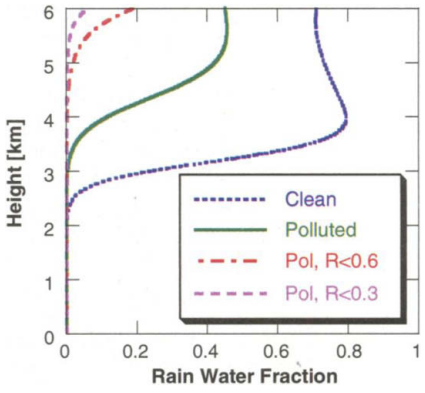

Fig. 5. The same as Fig. 4D, but with cloud base updraft increased from 1 m s^{-1} in Fig. 4 to 3 m s^{-1} here.

most susceptible to the impact of pollution aerosols on their albedo (*27*). However, the findings here suggest that this susceptibility does not translate into large sensitivity to anthropogenic land-based aerosols as currently believed, for two reasons: (i) Aerosols in a cloudy marine boundary layer are deposited quickly by cloud processes; and (ii) when pollution aerosols manage to interact with clouds over the sea, the sea salt reduces the supersaturation and hence the droplet concentrations and cloud albedo. These are likely causes for the larger cloud drop r_{eff} for the same aerosol index over the ocean as compared to land (*28*), recently observed by satellite, which has been unexplained until now.

References and Notes

1. S. K. Satheesh, V. Ramanathan, *Nature* **405**, 60 (2000).
2. D. Rosenfeld, *Geophys. Res. Lett.* **26**, 3105 (1999).
3. D. Rosenfeld, *Science* **287**, 1793 (2000).
4. D. Rosenfeld, Y. Rudich, R. Lahav, *Proc. Natl. Acad. Sci. U.S.A.* **98**, 5975 (2001).
5. G. A. McFarquhar, A. Heymsfield, *J. Geophys. Res.* **106**, 28653 (2001).
6. D. Rosenfeld D., G. Gutman, *Atmos. Res.* **34**, 259 (1994).
7. A. P. Khain, D. Rosenfeld, A. Pokrovsky, *Geophys. Res. Lett.* **28**, 3887 (2001).
8. D. A. Hegg, Y. J. Kaufman, *J. Geophys. Res.* **103**, 5671 (1998).
9. D. Rosenfeld, I. M. Lensky, *Bull. Am. Meteorol. Soc.* **79**, 2457 (1998).
10. W. A. Cooper, R. T. Bruintjes, G .K. Mather, *J. Appl. Meteorol.* **36**, 1449 (1997).
11. C. D. O'Dowd, J. A. Lowe, M. H. Smith, A. D. Kaye, *Q. J. R. Meteorol. Soc.* **125**, 1295 (1999).
12. G. Feingold, W. R. Cotton, S. M. Kreidenweis, J. T. Davis, *J. Atmos. Sci.* **56**, 4100 (1999).
13. Y. Yin, Z. Levin, T. G. Reisin, S. Tzivion, *Atmos. Res.* **53**, 91 (2000).
14. Z. Levin, E. Ganor, V. Gladstein, *J. Appl. Meteorol.* **35**, 1511 (1996).
15. Y. Rudich, D. Rosenfeld, O. Khersonsky, *Nature*, in press.
16. M. A. LeMone, E. J. Zipser, *J. Atmos. Sci.* **37**, 2458 (1980).
17. C. Lucas, E. J. Zipser, M. A. LeMone, *J. Atmos. Sci.* **51**, 3183 (1994).
18. HYSPLIT4 is the Hybrid Single-Particle Lagrangian Integrated Trajectory model. Web address: http://www.arl.noaa.gov/ready/hysplit4.html (NOAA Air Resources Laboratory, Silver Spring, MD, 1997).
19. J. Lelieveld *et al.*, *Science* **291**, 1031 (2001).
20. A. H. Woodcock, *J. Meteorol.* **10**, 362 (1953).
21. N. Sugimoto *et al.*, *J. Mar. Meteorol. Soc. Jpn.*, **76**, 93 (2000).
22. B. A. Albrecht, *Science* **245**, 1227 (1989).
23. A. S. Ackerman, O. B. Toon, P. V. Hobbs, *Science* **262**, 226 (1993).
24. D. Rosenfeld, W. L. Woodley, *Meteorol. Monogr.*, in press.
25. D. Rosenfeld, C. W. Ulbrich, *Meteorol. Monogr.*, in press.
26. A. P. Khain, M. Ovtchinnikov, M. B. Pinsky, A. Pokrovsky, H. Krugliak, *Atmos. Res.* **55**, 159 (2000).
27. S. Twomey, *J. Atmos. Sci.* **34**, 1149 (1977).
28. F. M. Breon, D. Tanre, S. Generoso, *Science* **295**, 834 (2002).

29. The authors thank V. Ramanathan for provoking this study by asking "What happens to the air pollution over the Indian Ocean as it goes into the ITCZ?" This study was funded by the Israeli Space Agency and by the Israeli Water Commission. Funding was also provided by project EURAINSAT, a shared-cost project (contract EVG1-2000-00030) cofunded by the Research Directorate General of the European Commission within the research and technological development activities of a generic nature of the Environment and Sustainable Development subprogram (5th Framework Programme).

Supporting Online Material

www.sciencemag.org/cgi/content/full/1073869/DC1
Figs. S1 to S8
References

13 May 2002; accepted 5 August 2002
Published online 15 August 2002;
10.1126/science.1073869
Include this information when citing this paper.

REPORTS

High Carrier Mobility in Single-Crystal Plasma-Deposited Diamond

Jan Isberg,[1]* Johan Hammersberg,[1] Erik Johansson,[1] Tobias Wikström,[1] Daniel J. Twitchen,[2] Andrew J. Whitehead,[2] Steven E. Coe,[2] Geoffrey A. Scarsbrook[2]

Room-temperature drift mobilities of 4500 square centimeters per volt second for electrons and 3800 square centimeters per volt second for holes have been measured in high-purity single-crystal diamond grown using a chemical vapor deposition process. The low-field drift mobility values were determined by using the time-of-flight technique on thick, intrinsic, freestanding diamond plates and were verified by current-voltage measurements on *p-i* junction diodes. The improvement of the electronic properties of single-crystal diamond and the reproducibility of those properties are encouraging for research on, and development of, high-performance diamond electronics.

The desire for electronic devices with higher power throughput, wider frequency bandwidth, and higher operational temperatures is driving research and development of new semiconductors. One such area is wide–band-gap materials. Diamond is extreme in this group of materials, which includes SiC, ZnO, and GaN, having a direct band gap of 7.5 eV, an indirect gap of 5.5 eV, and a room-temperature thermal conductivity in excess of 2000 W/mK. Diamond electronic devices, such as power diodes and high-frequency field-effect transistors, are expected to deliver outstanding performance because of the material's excellent intrinsic properties, such as high carrier mobilities and high breakdown field (*1*, *2*). However, the development of diamond electronics has been hampered by several problems, such as a lack of shallow dopants, heteroepitaxy as a route to large-area single-crystal growth, low crystal quality, and poor consistency of synthetic material. Nevertheless, interesting devices have been made; for example, Koizumi and co-workers have recently realized an ultraviolet light–emitting *p-n* diode in diamond (*3*).

Synthetic diamond has been produced for the past 50 years with high-pressure high-temperature (HPHT) technology and more recently by chemical vapor deposition (CVD). CVD offers a process for producing high–crystalline quality diamond under tightly controlled conditions. Although high-quality polycrystalline diamond with many properties that approach those of the best natural diamonds is now commercially available, the presence of grain boundaries impedes electronic performance, so that the only option for the most demanding applications is single-crystal CVD diamond. Despite more than 10 years of intensive research in this area, the best material suitable for electronic applications that has been reported is thin layers (typically $\ll$100 μm) having electronic properties, such as carrier mobility and lifetime, similar to those measured in specially selected natural type IIa diamond (*4*). Reported room-temperature values of carrier mobility (μ) in type IIa diamond are typically in the range of 2000 to 2800 cm^2/Vs for electrons and 1800 to 2100 cm^2/Vs for holes. This is the case for both Hall (*5*, *6*) and drift (*7*, *8*) mobility measurements. In homoepitaxial boron-doped CVD diamond, Yamanaka *et al.* (*9*) have measured a Hall hole mobility of 1840 cm^2/Vs. Improvement in electronic properties such as carrier mobility and lifetime can be directly related to enhanced crystalline quality and reduced defect

[1]ABB Group Services Center, Corporate Research, Nanotechnology and Innovative Materials Group, Västerås, Sweden. [2]De Beers Industrial Diamonds, King's Ride Park, Ascot, UK.

*Present address: Division for Electricity Research, Box 539, S-751 21 Uppsala University, Sweden. E-mail: jan.isberg@angstrom.uu.se